

Quantifying Heterogeneity of Individual Organelles in Mixed Populations via Mass Cytometry

Heather M. G. Brown,¹ and Edgar A. Arriaga^{1*}

University of Minnesota, Twin Cities

¹Department of Chemistry, 207 Pleasant St SE, Minneapolis, MN 55455

*Corresponding Author

TABLE OF CONTENTS

Table S-1. Metal-Labeled Antibody Panel Characterization.....	2
Figure S-1. Intra-assay precision assessed via technical replicates.....	3
Figure S-2. Organelle event gating strategy.....	4
Figure S-3. Low signal threshold calculations.....	5
Table S-2. Calculated Low Signal Threshold Values.....	6
Figure S-4. Characterization of the Abundance of Phenotypically Unique Organelle Populations.....	7
Figure S-5. Comparison of the Number of Specific Marker Antibodies Bound to Each Organelle Type.....	8
Figure S-6. Multi-dimensional t-SNE Analysis of Organelle from Liver Tissue.....	9
Figure S-7. Multi-dimensional t-SNE Analysis of Organelles from Skeletal Muscle Tissue.....	10

Table S-1. Metal-Labeled Antibody Panel Characterization. The following antibodies were metal labeled and further characterized to quantify the average number of metal ions chelated by each polymer-antibody ligand.

Target	Metal Isotope	Host Isotype	Clone	# Metal Ions / Antibody	Antibody Vendor & P/N
TOMM22	¹⁵⁴ Sm	Mouse, IgG2a κ	4G4	56	Sigma, WH0056993M1
LAMP2	¹⁶² Dy	Rabbit, IgG	poly	78	Sigma, L0668
LC3	¹⁴² Nd	Rabbit, IgG	poly	76	Novus, NB100-2220
Rabbit Isotype	¹⁷¹ Yb	Rabbit, IgG	poly	62	Invitrogen, 026102
Mouse Isotype	¹⁴¹ Pr	Mouse, IgG	poly	58	Invitrogen, 026502

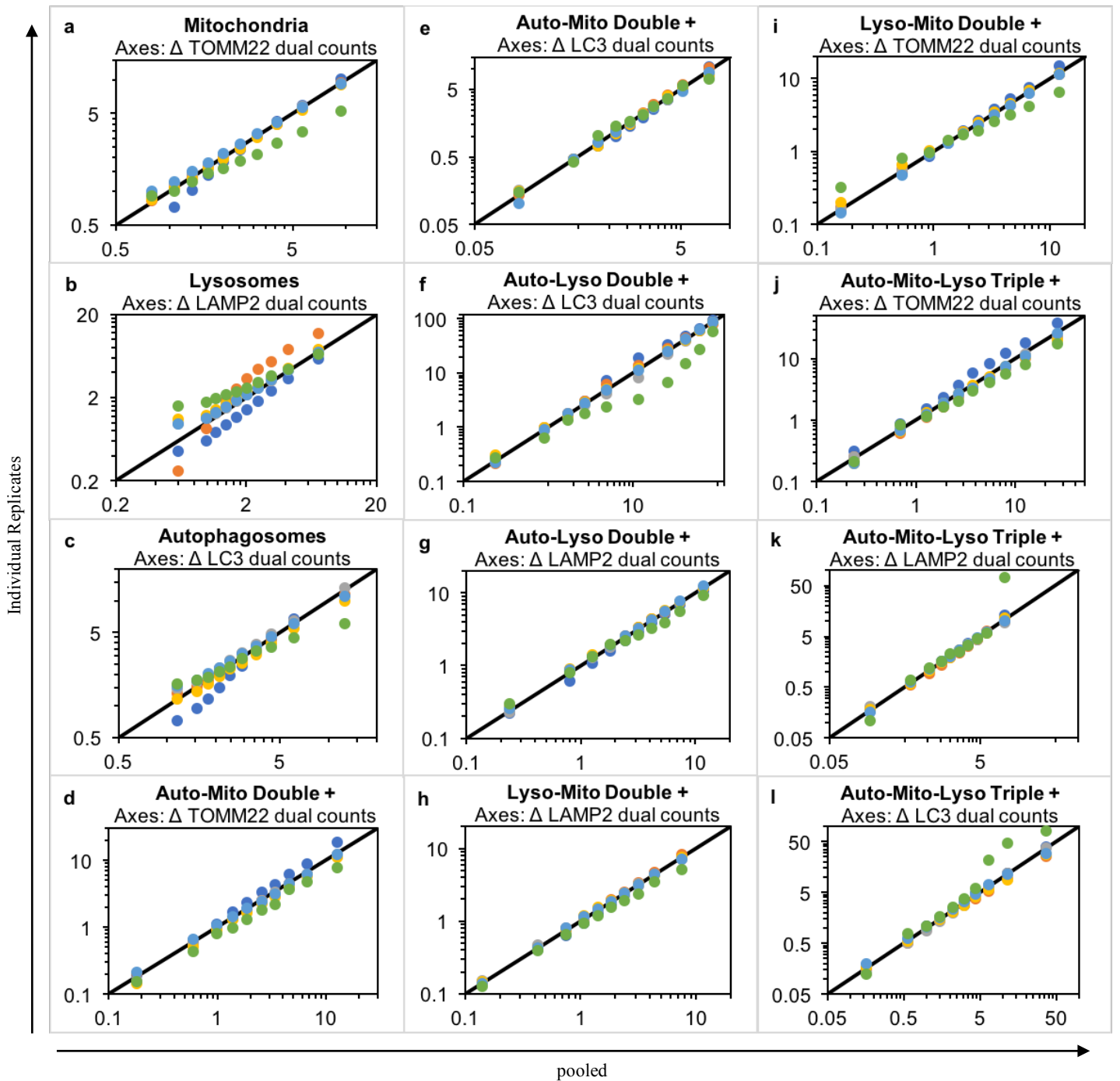


Figure S-1. Intra-assay precision assessed via technical replicates. Intra-assay precision was assessed via acquisition of six technical replicates spaced over thirteen hours of data acquisition. Phenotypically unique organelle distributions from each replicate were binned into deciles and plotted on a quantile-quantile plot. If the replicate distribution is similar to the pooled distribution, the plot will approach the $x=y$ line. Scales vary in each panel based on the marker represented. Replicates (shown as different colored series) show minimal deviation from $x=y$, indicating that all replicate distributions are similar enough to originate from the same pooled distribution. Where deviations do occur (i.e. panels a, b, c f, i-l), series that deviate were data collected at the beginning (replicate 1, dark blue) or end (replicate 6, green), which is not surprising because these measurements were done 13 hours apart, indicating potential limits in sample or instrument stability. Other replicates were measured consecutively 5 hours after replicate one and 5 hours prior to the last replicate. These observations apply to all phenotypically unique organelle populations, including: a) mitochondria (TOMM22+), b) lysosomes (LAMP2+), c) LC3+ autophagy organelles – mitochondria (LC3+TOMM22+), d-e) LC3+ autophagy organelles – lysosomes (LC3+LAMP2+), f-g) LC3+ autophagy organelles – lysosomes (LC3+LAMP2+), h-i) lysosomes – mitochondria (LAMP2+TOMM22+), and j-l) LC3+ autophagy organelles – mitochondria – lysosome (TOMM22+LAMP2+LC3+). The number of organelles in each technical replicate were as follows: replicate 1, $n = 20,440$, dark blue (•); replicate 2, $n = 19,995$, orange (•); replicate 3, $n = 22,195$, gray (•); replicate 4, $n = 9,208$, yellow (•); replicate 5, $n = 22,410$, light blue (•); replicate 6, $n = 1,632$, green (•).

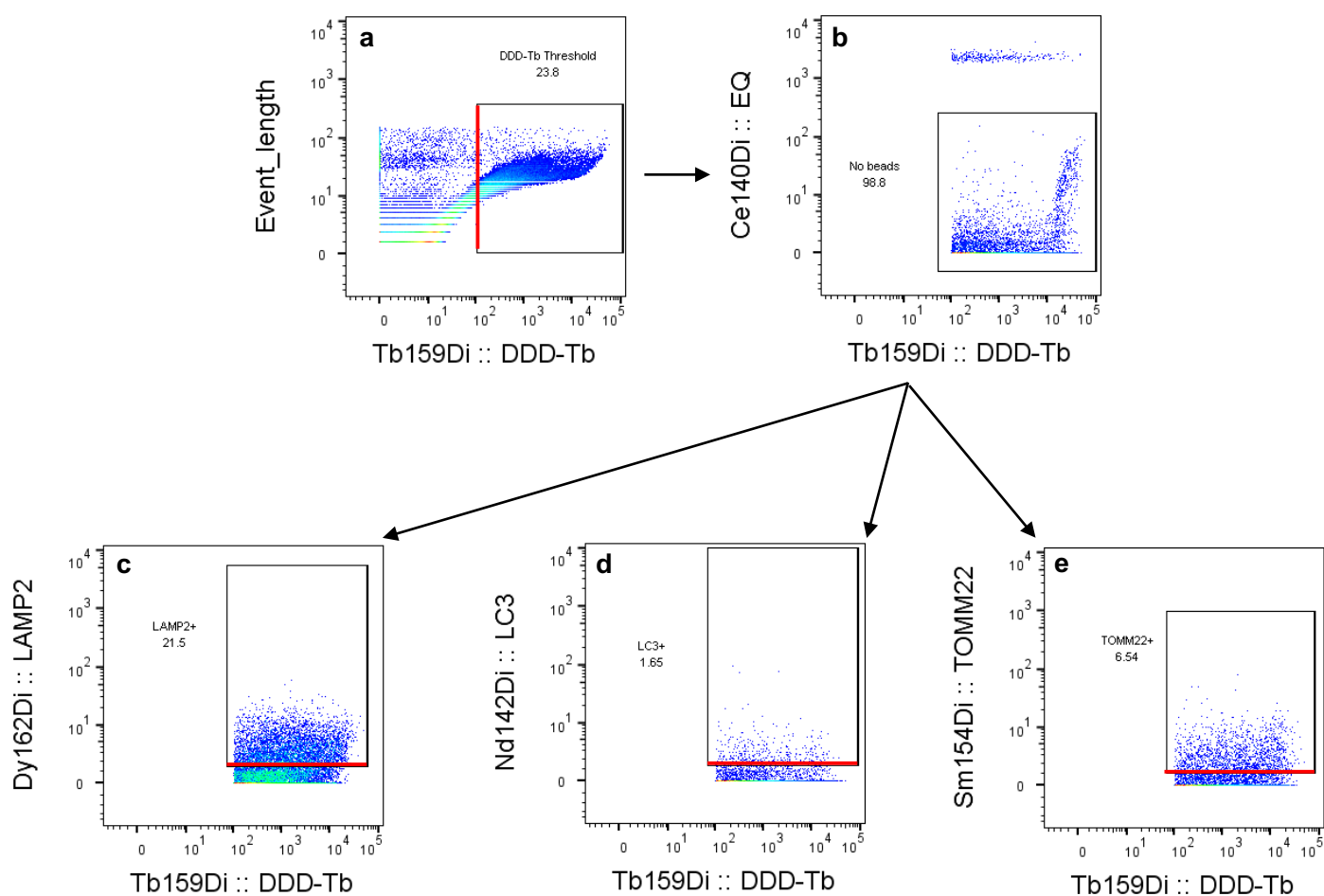


Figure S-2. Organelle event gating strategy. Calculated low signal threshold values used as lower bounds for phenotypic identification. The first two panels (a-b) show sequential gates: (a) application of DDD-Tb low signal threshold, (b) removal of EQ normalization bead – organelle aggregate events. The lower three panels show the application of the calculated lower signal threshold to phenotypically identify organelle events: c) LAMP2 (lysosome), d) LC3 (LC3+ organelles), e) TOMM22 (mitochondria).

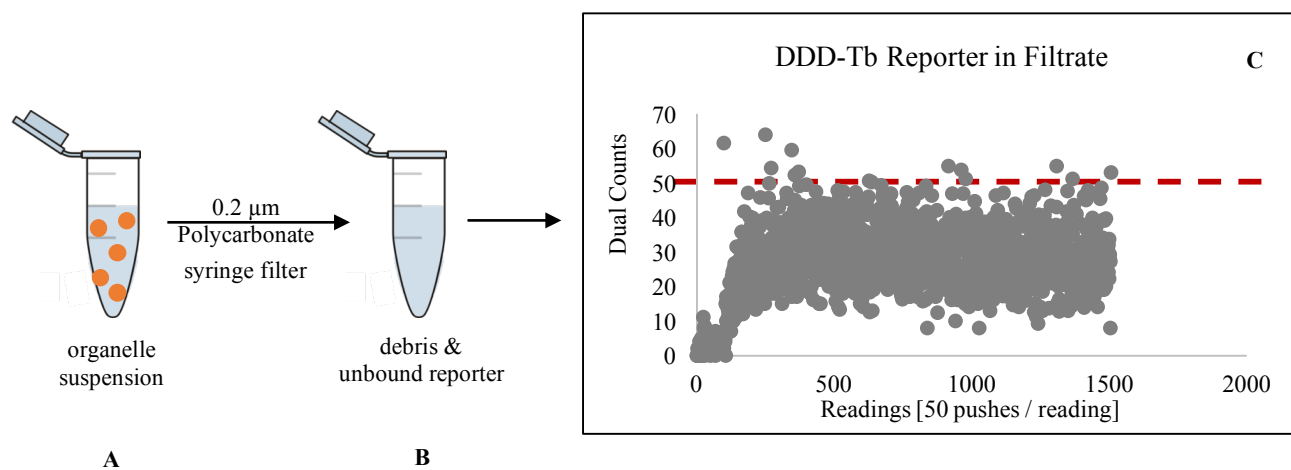


Figure S-3. Low signal threshold calculation. To set a low threshold for each monitored m/z channel, an aliquot of organelle suspension (A) was filtered through a 0.2 µm polycarbonate filter to remove most organelles. This results in a suspension of debris & unbound reporter (B), which was analyzed in solution mode on the CyTOF2. The low signal threshold (C) is calculated as the mean dual count signal in a given channel plus three times the standard deviation of the mean. This low signal threshold value was calculated over a stable range, typically 400-1400 readings.

Table S-2. Calculated Low Signal Threshold Value. A threshold value was calculated for each m/z value in each organelle sample. B = brain, L = liver, M = skeletal muscle, R1 = biological replicate, mouse 1, R2 = biological replicate, mouse 2.

Tissue - Replicate	Calculated low signal threshold value (DC signal)			
	¹⁴² Nd-LC3	¹⁵⁴ Sm-TOMM22	DDD- ¹⁵⁹ Tb	¹⁶² Dy-LAMP2
B-R1	0.5264	0.4218	8.2087	0.3114
B-R2	0.9078	0.6404	9.9606	0.6100
L-R1	0.4400	0.7324	26.3693	0.8331
L-R2	0.7978	0.6900	15.9290	1.4507
M-R1	0.7324	0.7189	8.9970	0.4163
M-R2	1.0010	0.7720	12.9580	0.7039

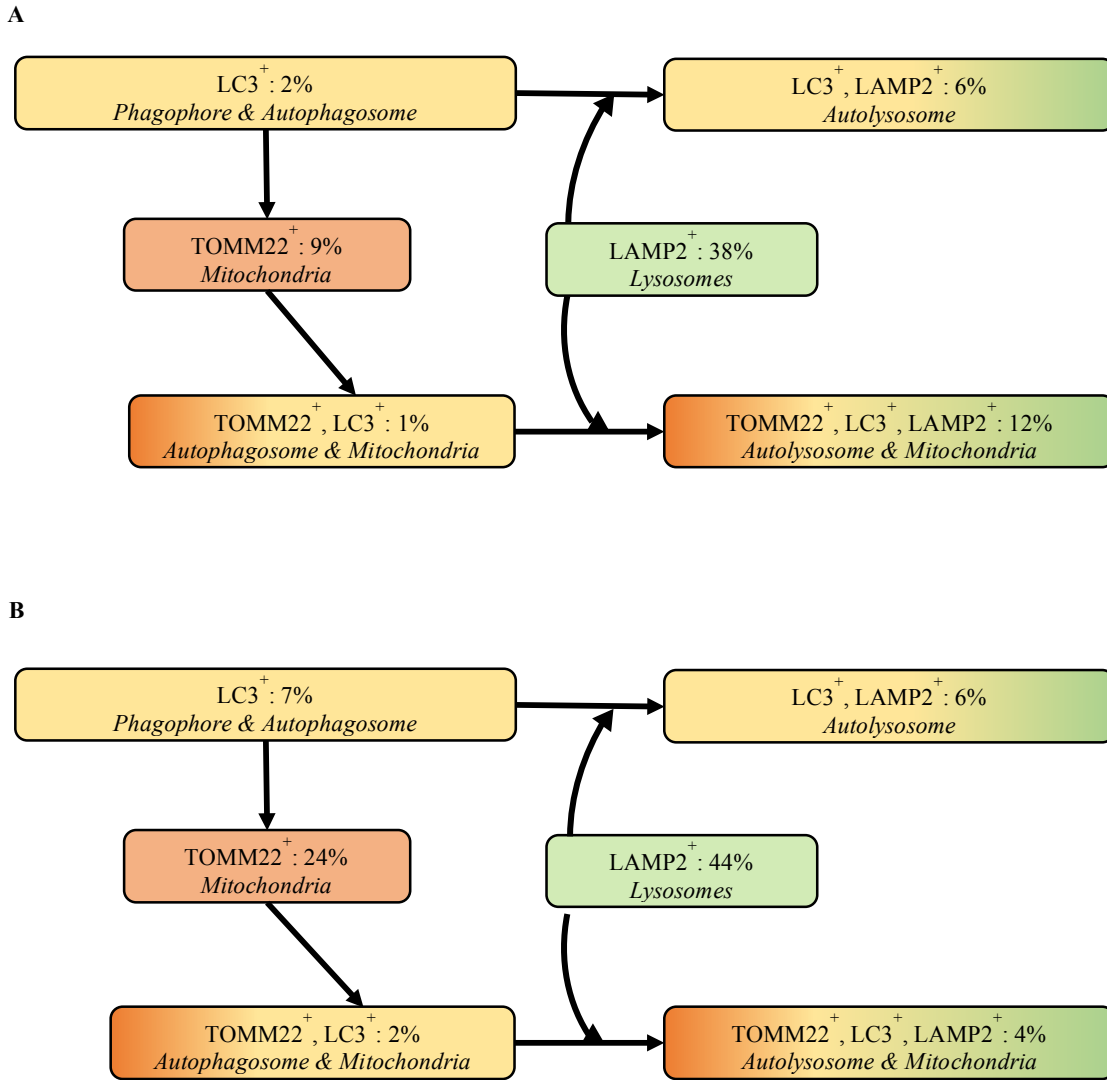


Figure S-4. Characterization of the Abundance of Phenotypically Unique Organelle Populations. The percent contribution from each phenotypically unique organelle type to the total number of identified organelles was calculated for liver (A) and skeletal muscle (B) tissues. Tissue-specific differences in organelle content are expected due to differences in cellular function of the organelle types in each tissue.

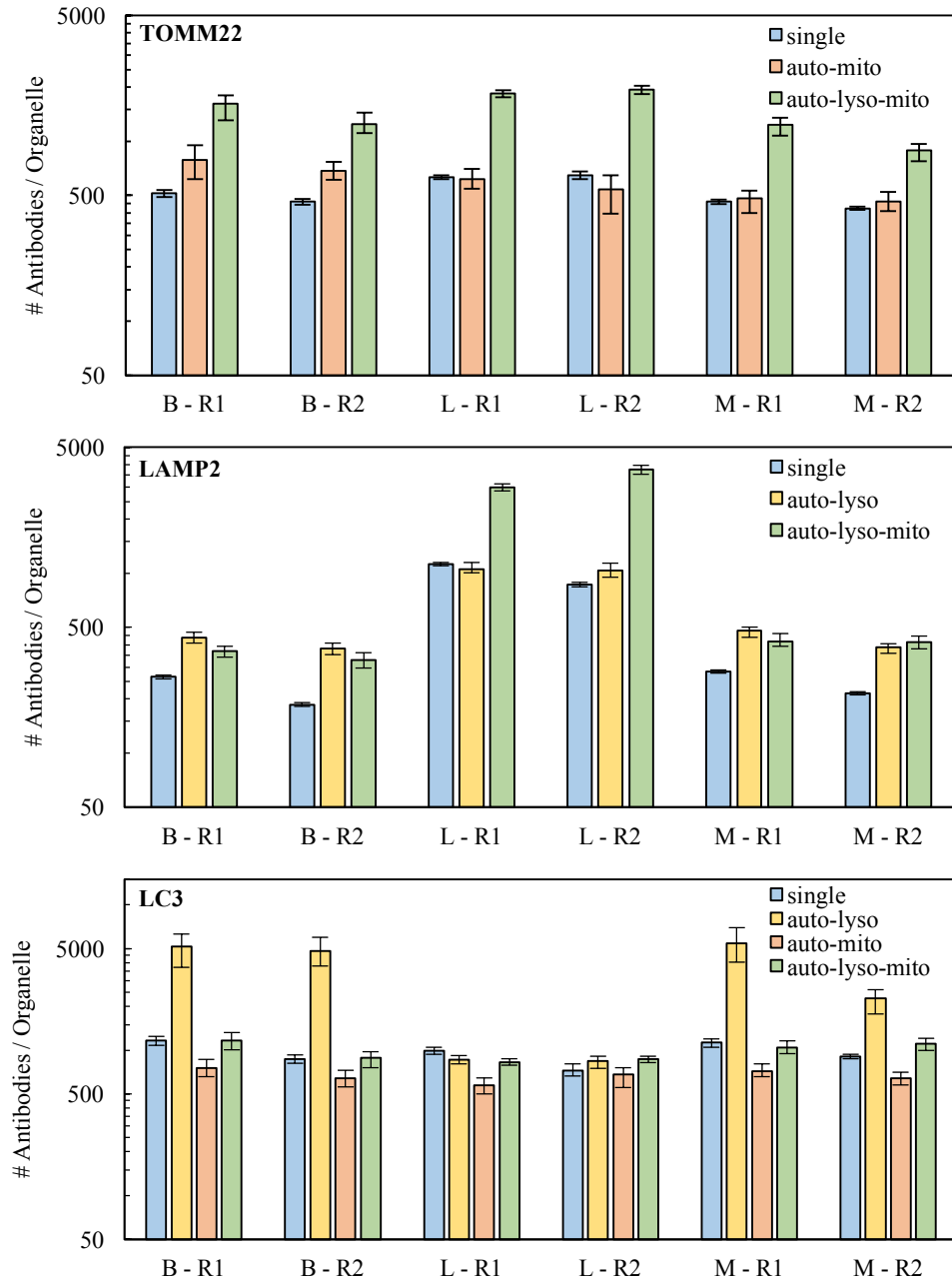


Figure S-5. Comparison of the number of specific marker antibodies bound to each organelle type. The calculated number of specific marker antibodies detected per organelle generally increases with progression to late autophagic organelles. The increase in markers is generally accompanied by an increase in the number of DDD-Tb molecules per detected organelle, which suggests an increase in total membrane volume. The number of specific marker antibodies per organelle was normalized to the DDD-Tb dual count signal, and the resulting plots are shown in Figure 2a-c. Error represented as 95% confidence intervals of the median. B = brain, L = liver, M = skeletal muscle, R1 = biological replicate, mouse 1, R2 = biological replicate, mouse 2. See Figure S-4 for corresponding analysis of liver and skeletal muscle tissue.

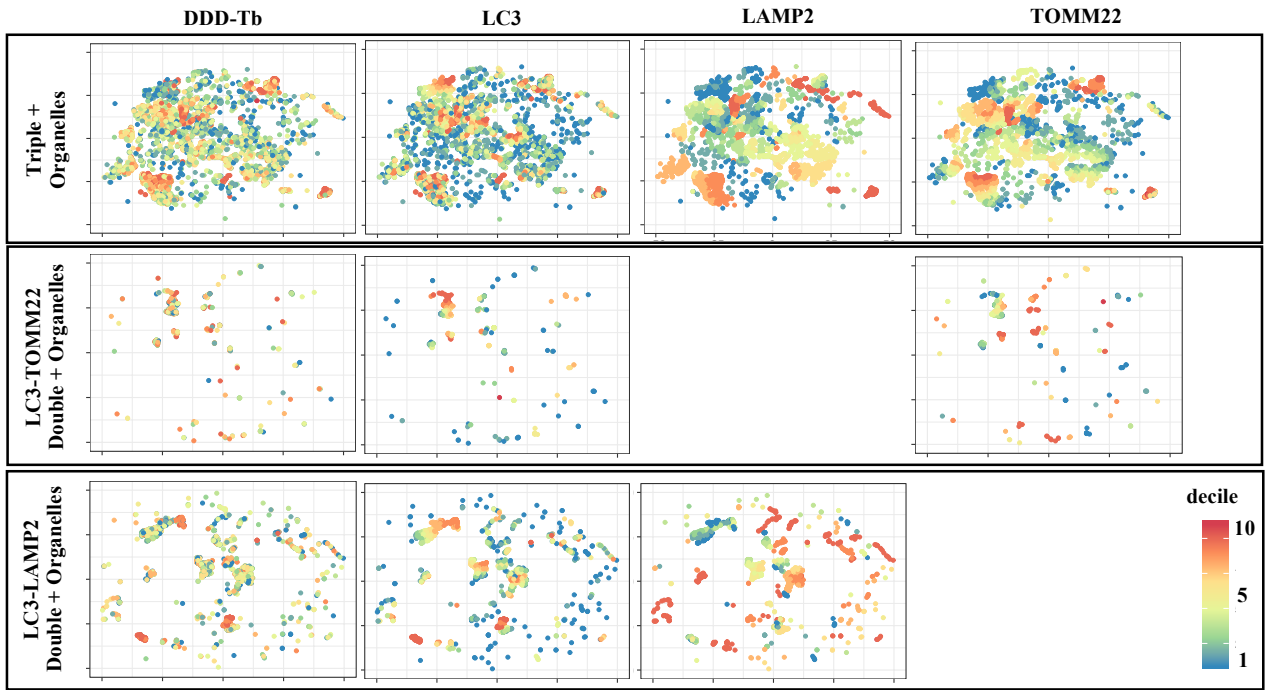
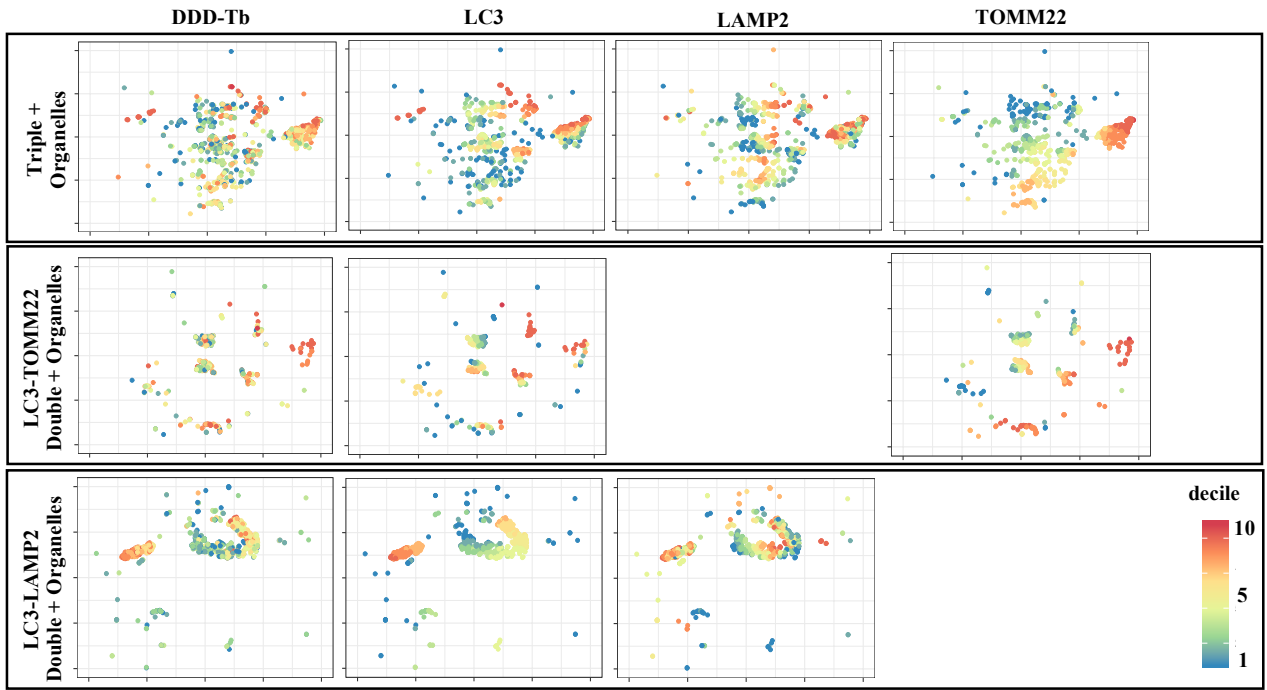


Figure S-6. Multi-dimensional t-SNE analysis of organelles from liver. t-SNE plots from murine liver tissue show phenotypically identified populations of organelles. Distributions of specific markers on individual organelles were binned into deciles and color-coded according to their assigned decile. Wide variation in color across specific markers in t-SNE plots indicate heterogenous sub-populations, which may have significantly different function. Triple + organelles represent autolysosomes associated with mitochondria, while LC3-TOMM22 double + organelles represent autophagosomes associated with mitochondria, and LC3-LAMP2 double + organelles represent autolysosomes.



Supplementary Figure S-7. Multi-dimensional t-SNE analysis of organelles from skeletal muscle. t-SNE plots from murine skeletal muscle tissue show phenotypically identified populations of organelles. Distributions of specific markers on individual organelles were binned into deciles and color-coded according to their assigned decile. Wide variation in color across specific markers in t-SNE plots indicate heterogeneous sub-populations, which may have significantly different function. Triple + organelles represent autolysosomes associated with mitochondria, while LC3-TOMM22 double + organelles represent autophagosomes associated with mitochondria, and LC3-LAMP2 double + organelles represent autolysosomes.